JOC The Journal of Organic Chemistry

Article

pubs.acs.org/joc

Mechanistic Insights into the Vanadium-Catalyzed Achmatowicz Rearrangement of Furfurol

Yining Ji,[†] Tamas Benkovics,*[,‡] Gregory L. Beutner,[‡] Chris Sfouggatakis,[‡] Martin D. Eastgate,[‡] and Donna G. Blackmond*[,†]

[†]Department of Chemistry, The Scripps Research Institute, 10550 North Torrey Pines Road, La Jolla, California 92037, United Sates

[‡]Chemical Development, Bristol-Myers Squibb, One Squibb Drive, New Brunswick, New Jersey 08903, United States

Supporting Information

ABSTRACT: The Achmatowicz rearrangement is a powerful method for the construction of pyranones from simple furan derivatives. Here, we describe the development of improved reaction conditions and an interrogation into the fate of the metal center during this interesting transformation. The reaction to form the synthetically important lactol, 6-hydroxy-2*H*-pyran-3(6*H*)-one (**3**), proceeds cleanly in the presence of *tert*-butyl hydroperoxide (TBHP, **2**) using low loadings of $VO(O^iPr)_3$ as catalyst. The nonaqueous conditions developed herein allow for easy isolation of product **3** and synthetically important derivatives, a key advantage of this new protocol. Detailed experimental, spectroscopic, and kinetic studies along with kinetic modeling of the catalytic cycle support a positive-order dependence in both furfurol and TBHP concentrations, first-order dependence in catalyst ($VO(O^iPr)_3$), and a *negative* dependence on the 2-methyl-2-propanol (**4**) concentration. ^{51}V-NMR spectroscopic studies revealed that 2-methyl-2-propanol (**4**) competes with substrates for binding to the metal center, rationalizing its inhibitory effect.

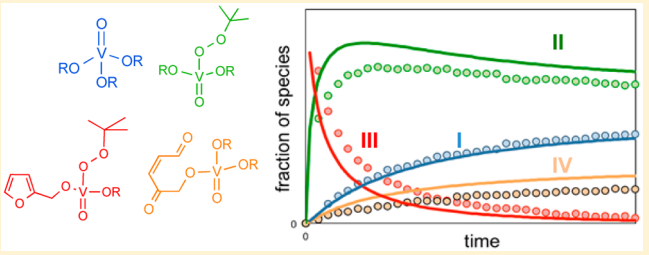

INTRODUCTION

The Achmatowicz rearrangement of furans to provide substituted pyranones is a powerful method for the preparation of these densely functionalized building blocks.[1] The transformation is widely used in the synthesis of carbohydrates[2] as well as other natural products.[3] Reagents such as *m*-chloroperoxybenzoic acid[4] or bromine−MeOH[5] have been routinely used for this transformation but suffer from significant drawbacks from the standpoint of atom economy, process efficiency, and ease of product isolation.[6] More environmentally benign oxidants such as hydrogen peroxide have been utilized,[7] but the presence of water in these systems often results in serious challenges during isolation since many of these pyranone derivatives have significant water solubility. This is particularly true for the simplest product of this transformation (Scheme 1), 6-hydroxy-2*H*-pyran-3(6*H*)-one (**3**), generated from furfurol (**1**).

In the context of a recent program, we wished to find a more atom-economical and efficient method for the preparation of **3** from furfurol. Importantly, we desired conditions that would enable a facile isolation of the product, which meant eliminating water both in the reaction mixture and during the workup protocol. On the basis of literature reports,[8] it was clear that *tert*-butyl hydroperoxide (TBHP, **2**) was a competent oxidant for this transformation, functioning in an anhydrous medium that would allow for either the direct isolation of product **3** or its direct use in a subsequent transformation. In this report, we describe the development of a robust reaction and isolation method for the Achmatowicz rearrangement of furfurol using catalytic $VO(O^iPr)_3$ (Scheme 1), as well as mechanistic investigations based on a combination of kinetic analysis, ^{51}V-NMR spectroscopic identification of catalytic intermediates, and kinetic modeling to provide a more detailed understanding of this transformation.

Scheme 1. Achmatowicz Rearrangement of Furfurol

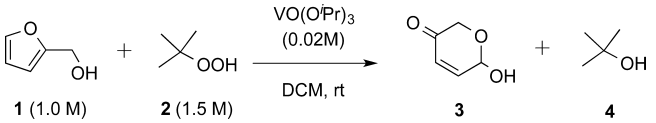

RESULTS AND DISCUSSION

In order to evaluate the performance of the Achmatowicz reaction, we decided to investigate a range of oxidants and vanadium catalysts. After optimization of the reaction, varying vanadium source ($VO(acac)_2$ vs $VO(O^iPr)_3$), oxidant (TBHP vs cumene hydroperoxide), solvent, temperature, and addition order, we were delighted to find that the oxidative rearrangement gave the desired product in good in-process yield (Scheme 2). Although detailed studies of temperature effects were not carried out, the reaction proceeds cleanly at

Received: November 19, 2014

© XXXX American Chemical Society

DOI: 10.1021/jo502641d
J. Org. Chem. XXXX, XXX, XXX−XXX

Scheme 2. Preparation of Compounds 3, 5, and 6

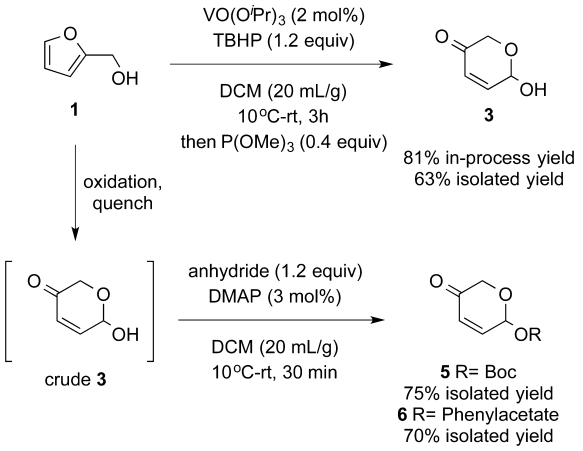

temperatures between 10 °C and room temperature. Additionally, lactol **3** could be isolated after quenching the residual oxidant with trimethylphosphite followed by a direct crystallization from heptanes/^{t}BuOH. Alternatively, the crude reaction mixture of **3** could be carried directly into an acylation step with various anhydrides to provide improved access to these useful synthetic building blocks as crystalline solids.

Although the vanadium-catalyzed furfurol oxidation produced **3** in a reproducible fashion, the reaction appeared to stall despite an initial rapid reaction rate. In order to understand this phenomenon in more detail, we undertook a detailed kinetic study of the VO(O^iPr)$_3$/TBHP system. FTIR spectroscopy was employed for continuous monitoring of the reaction. The formation of product **3** was monitored using the height of the peak at ca. 1708 cm^{-1}, and consumption of furfurol (**1**) was followed by a multicomponent method (concIRT). Validation of this in situ method was carried out by comparison to an alternative method; in this case, ^{1}H NMR spectroscopy, where an excellent correlation was observed (Figure 1). To characterize the kinetic behavior of the system, a series of experiments was designed and performed (Table 1). Both the concentration dependence and the stability of the catalyst system could then be probed using the "different excess" and "same excess" protocols through reaction progress kinetic analysis (RPKA), respectively.[9]

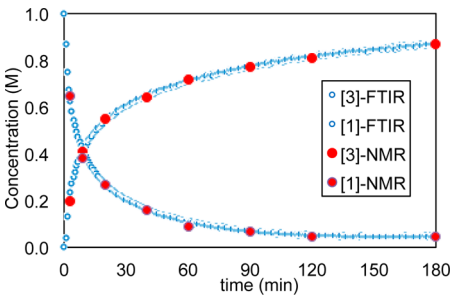

Figure 1. Comparison of temporal kinetic profiles monitored by FTIR and NMR spectroscopy of reactant **1** and product **3** for the reaction of Scheme 1.

Comparison of kinetic profiles under standard and "same excess" conditions is a technique that has been employed previously to probe catalyst robustness. Comparison of two or more "different excess" experiments can also provide information about the reaction order in substrate concentration. Both protocols employ a simple graphical manipulation of the reaction data to extract this information.

Table 1. Reaction Conditions[a]

reaction	$[\mathbf{1}]_0$ (M)	$[\mathbf{2}]_0$ (M)	comment
a	1.0	1.5	standard
b	0.5	1.0	same excess
c	0.5	1.5	different excess
d	0.5	1.0	0.4 M product **3** addition
e	0.5	1.0	0.4 M product **4** addition
f	1.0	1.5	0.5 M ^{i}PrOH addition
g	1.0	1.5	1.0 M ^{i}PrOH addition
h	1.0	1.5	VO(O^tBu)$_3$ catalyst

[a]All reactions run in DCM at room temperature using 0.02 M VO(O^iPr)$_3$ (VO(O^tBu)$_3$ for reaction **h**) as catalyst.

Figure 2 plots the concentration profiles for two "same excess" experiments (reactions **a** and **b**, Table 1) designed to test catalyst stability. As the dotted lines show, the concentrations of furfurol (**1**) and TBHP (**2**) at the beginning of reaction **b** (red circles) are identical to those of reaction **a** (blue circles) after ca. 4.5 min of reaction; i.e., reaction **b** is started with a composition mimicking reaction **a** after 4.5 min. Comparison of the profiles of these two reactions is then possible by shifting the curve from reaction **b** to the appropriate time on the *x*-axis. After this transformation, identical reaction profiles should be expected if the activity of the catalyst remains constant throughout the reaction. However, it is clear that reaction **b** proceeds significantly faster than reaction **a**. The lack of overlay of these "time adjusted" kinetic profiles suggests that some process, other than the intrinsic kinetics related to the temporal substrate concentrations of [**1**] and [**2**], contributes to the observed rate changes.

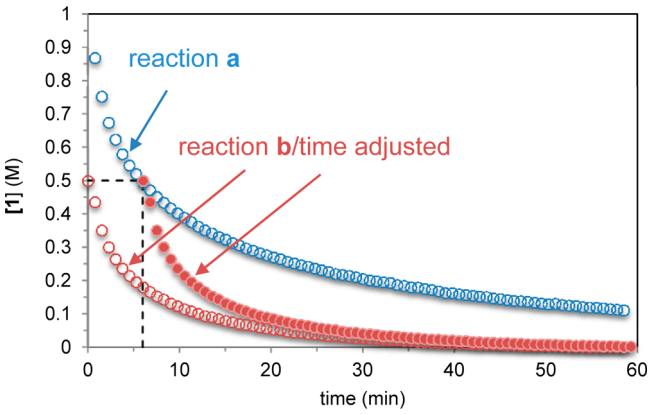

Figure 2. Concentration of substrate **1** as a function of time for reaction **a** compared with "same excess" reaction **b** as noted in Table 1. The time-adjusted profile for reaction **b** has the same [**1**] and [**2**] as reaction **a** has at the point marked by the dotted lines.

Two key differences exist between the reactions **a** and **b** at the point marked by the dotted arrows shown in Figure 2; (i) the catalyst in reaction **a** has undergone several turnovers, while reaction **b** employs fresh catalyst, and (ii) reaction **a** is at ca. 50% conversion and contains 0.4 M **3** and **4** ^{t}BuOH while reaction **b** contains only substrate and catalyst. Thus, two main possibilities exist for the lack of overlay between curves **a** and **b**, from the time-adjusted point onward: either the concentration of catalyst in the productive cycle is decreasing through

DOI: 10.1021/jo502641d
J. Org. Chem. XXXX, XXX, XXX−XXX

irreversible deactivation or a reaction product is inhibiting catalyst turnover.

Product inhibition can be independently tested by carrying out a reaction under the conditions of reaction **b** while adding the appropriate quantity of products **3** and/or **4** to mimic the time-adjusted point. When the conditions of reaction **b** were repeated in the presence of 0.4 M **3** (Figure 3, reaction **d**), excellent superposition was observed, suggesting that lactol **3** does not interfer with the active catalysts turnover.

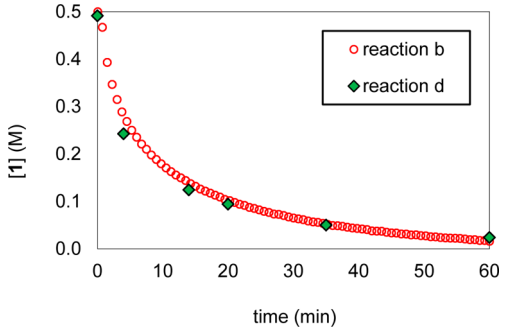

Figure 3. Effect of product **3** concentration on the temporal concentration profile of reaction **b**. Reaction **d** includes product **3** added to match its concentration of reaction **a** at the point of the time adjustment. Reaction **d** monitored using NMR spectroscopy.

In contrast, when the conditions of reaction **b** were repeated in the presence of 0.4 M **4** (Figure 4, reaction **e**), a slower

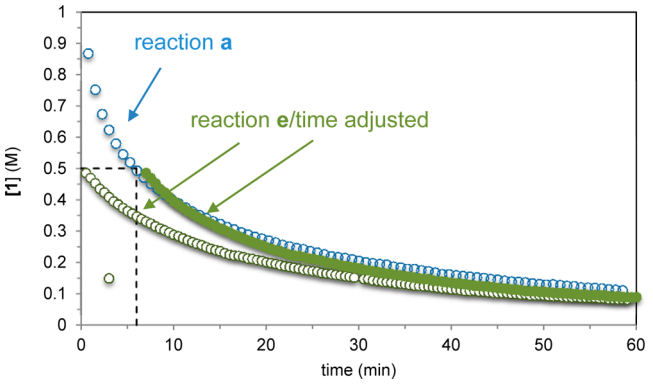

Figure 4. Concentration of substrate **1** as a function of time for reaction as compared to "same excess" conditions reaction **e**, with product **4** added to a concentration close to that of reaction **a** at the point of the time adjustment.

reaction was observed. Good superposition of reaction **e** was observed with standard reaction (profile **a**), demonstrating that the two reactions exhibit similar rates and suggesting that the catalyst system is sensitive to ^{t}BuOH inhibition. In addition, the reasonable overlay of these two profiles suggests that other catalyst deactivation processes are likely not as significant as alcohol inhibition under these conditions. The kinetic behavior appears robust, consistent with the vanadium catalyst remaining viable in the reaction medium throughout the reaction.

Having confirmed the inhibitory effect of the alcohol byproduct, 2-methyl-2-propanol (**4**), as well as the absence of any significant irreversible catalyst deactivation, we employed the "different excess" protocol of RPKA to probe the reaction orders in substrates [**1**] and [**2**]. The standard RPKA analysis involves consideration of the data in the form of reaction rate as a function of concentration. The "power-law" form of the rate expression can be represented by eq 1:

$$\text{rate} = k_{\text{obs}}[\mathbf{1}]^m[\mathbf{2}]^n[\mathbf{4}]^p \quad (1)$$

Normalization of the rate by $[\text{TBHP}]^n[^t\text{BuOH}]^p$ is shown as eq 2:

$$\frac{\text{rate}}{[\mathbf{2}]^n[\mathbf{4}]^p} = k_{\text{obs}}[\mathbf{1}]^m \quad (2)$$

The power−law values for reaction orders m, n, and p are thus obtained from RPKA plots of eq 2 for multiple data sets, with the function to the left of the equal sign plotted as the y-axis and the function $[\mathbf{1}]^m$ on the x-axis. Correctly chosen values for m, n, and p would therefore produce straight line correlations exhibiting "overlay" for a set of kinetic data from reactions carried out under "same excess", "different excess", and product added conditions. As illustrated in Figure 5, a

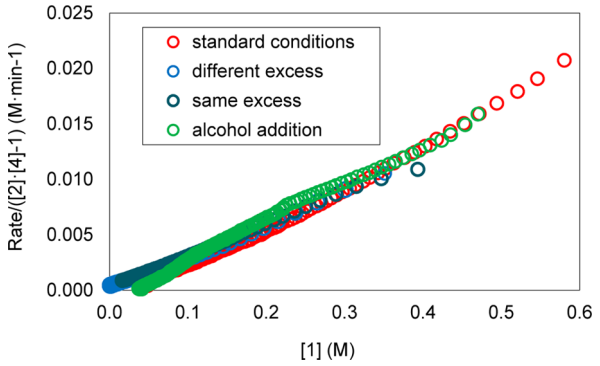

Figure 5. RPKA plot of the function shown in eq 2 with m = 1, n = 1, p = −1 for reaction entries **a**, **b**, **c**, and **e** of Table 1.

straight line with overlay between the four experimental profiles is obtained with m = 1, n = 1, and p = −1. The linearity confirms that the reaction is approximately first order in [**1**] (m = 1), while the overlay between the profiles suggests that the reaction exhibits an approximate first-order kinetic response (n = 1) to substrate [**2**] and a negative first-order response (p = −1) to [**4**]. A demonstration of the effect on "overlay" by other choice of reaction orders m, n, and p is given in the Supporting Information.

With an understanding of the orders of the different species in solution, we wished to gain more knowledge on the inhibitory effect of ^{t}BuOH and therefore sought an alternative technique that could provide more direct information on the catalytic species. Thus, ^{51}V NMR spectroscopy was employed to probe the structural basis of the inihibitory effect of ^{t}BuOH on the reaction. The ^{51}V isotope is perfectly suited to this task due to the high natural abundance of this nucleus (N = 99.76%, I = 7/2) and its high relative receptivity compared to ^{1}H (0.381).[10] This technique has been widely used to study ligand-exchange processes occurring at vanadium(V) atoms and is sensitive to subtle changes in ligand structure due to the wide chemical shift range for this nucleus (2000 ppm).[11] We hypothesized that this technique could allow for direct observation of the catalytic species in solution and provide further insight into the inhibition process as well as the overall reaction mechanism.

First, the complexes formed from the interaction between $VO(O^{i}Pr)_3$ and ^{t}BuOH (**4**) were investigated (Figure 6). A mixture of $VO(O^{i}Pr)_3$ and 4 equiv of ^{t}BuOH (**4**) led to the

DOI: 10.1021/jo502641d
J. Org. Chem. XXXX, XXX, XXX−XXX

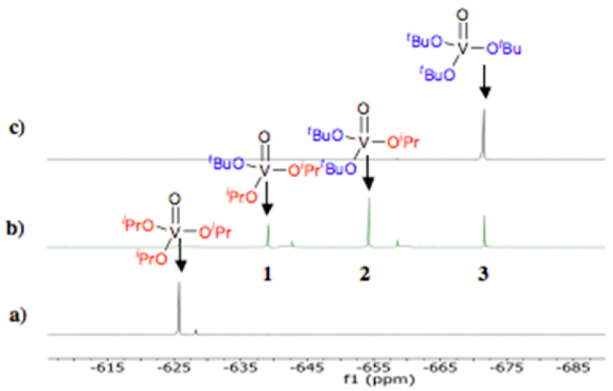

Figure 6. 131 MHz ^{51}V NMR spectra of a solution of (a) VO(O^iPr)$_3$, (b) VO(O^iPr)$_3$:^{t}BuOH (1:4), and (c) VO(O^tBu)$_3$. All of the spectra were recorded in CD_2Cl_2.

formation of three new complexes which were assigned as VO(O^iPr)$_2$(O^tBu), VO(O^iPr)(O^tBu)$_2$, and VO(O^tBu)$_3$ (−639, −654, and −671 ppm, respectively; Figure 6b). An authentic sample of VO(O^tBu)$_3$ was prepared[12] confirming its resonance at −671 ppm (Figure 6c). These experiments demonstrated a facile interchange between ^{i}PrOH and ^{t}BuOH at the vanadium-(V) center, an observation fully consistent with previous studies.[13,14]

Thus, we hypothesized that the inhibitory effect of ^{t}BuOH could be caused by one of two factors: (1) the new species [VO(O^iPr)$_2$(O^tBu), VO(O^iPr)(O^tBu)$_2$, and VO(O^tBu)$_3$] could possess different catalytic activities, or (2) binding of the substrate **1** with the catalyst is competitive with the other alcohols (e.g., IPA and ^{t}BuOH) in solution.

To assess the reactivity of 2-methyl-2-propanol containing catalysts against the triisopropoxide complex, we compared the activity of VO(O^tBu)$_3$ with VO(O^iPr)$_3$ under the standard conditions (Figure 7, Table 1, reactions **a** and **h**). The fact that

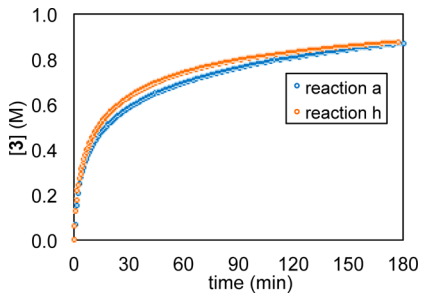

Figure 7. Comparison of the catalytic activity of VO(O^tBu)$_3$ (red circles) vs VO(O^iPr)$_3$ (blue circles).

the reaction rates were similar, regardless of catalyst structure, strongly argues against the possibility that the vanadium alkoxide complexes have different activities. Therefore, it appears that perhaps competitive binding of ^{i}PrOH, ^{t}BuOH (**4**), and substrate **1** to the metal center was the cause of the apparent loss in catalyst activity. If this is true, the addition of any alcohol should lead to a suppression of the reaction rate. This was confirmed experimentally by the addition of ^{i}PrOH, which produced a similar inhibitory effect to ^{t}BuOH (Table 1, reactions **f** and **g**, see the Supporting Information). Attempts to counter this inhibitory effect by using other hydroperoxides were unsuccessful. Cumyl alcohol from cumene hydroperoxide inhibited the reaction similarly to TBHP (**2**), while bulkier hydroperoxides were found to be insoluble under reaction conditions.

Given the large number of alkoxyvanadium(V) complexes that could be formed between the vanadium catalyst and the various alcohols in solution, we sought to understand this system in more detail. Therefore, the possible combinations of furfurol (**1**), TBHP (**2**), lactol **3**, and ^{t}BuOH (**4**) were explored in pairwise combination with VO(O^iPr)$_3$. Similar studies have been performed on other homogeneous vanadium-catalyzed oxidations in order to characterize key reaction intermediates.[15] Selected examples from our studies are shown in Figure 9, and full details of these structure elucidation experiments can be found in the Supporting Information. For easy reference, the values have been compiled in Table 2.

Having independently identified numerous vanadium complexes potentially formed in the reaction mixture, in situ ^{51}V NMR spectra were recorded over the course of the reaction under the standard conditions (Table 1, reaction **h**). For these studies, VO(O^tBu)$_3$ was chosen as the catalyst since simpler ^{51}V NMR spectra would be obtained in the absence of isopropoxide groups. Since the reactions of VO(O^iPr)$_3$ and VO(O^tBu)$_3$ proceeded at similar rates (see Figure 7), the conclusions of the study should prove general. By monitoring the reaction mixture under reaction conditions **h** by ^{51}V NMR over time, we were able to identify almost all observable species formed during the reaction mixture (Figure 8).

The kinetic profiles of these different vanadium species as a function of time are plotted in Figure 9 along with fractional conversion. At low conversions, the precatalyst VO(O^tBu)$_3$ (**I**, Table 2 and blue circles, Figure 9) is a minor species with the dominant species being the complex VO(O^tBu)(OO^tBu)-(furfurol) (**III**, Table 2, and red circles). As the reaction proceeds, **III** rapidly gives way to VO(O^tBu)$_2$(OO^tBu) (**II**, Table 2, and green circles, Figure 9). The concentration of a product-bound complex (**IV**, Table 2, and beige circles) and the ^{t}BuOH-bound complex **I** (blue circles) increases at higher conversion. The formation of the oxidant byproduct **4** is known to inhibit catalyst activity and is consistent with these results.[16] Computational studies have also described the role of oxidant byproducts in the complex equilibria involved in the binding of substrate to the catalyst's metal center.[17]

These results led us to propose the following reaction mechanism (Scheme 3) which best fits the observed species and kinetic data. Catalyst activation occurs via displacement of one alcohol group on precatalyst species **I** by TBHP (**2**) to provide entry into the catalytic cycle at species **II**.[18] Displacement of a second alcohol by binding of furfurol (**1**) then occurs, leading to formation of **III**. Complex **III** undergoes rate-determining, intramolecular oxidation in analogy to the epoxidation of allylic alcohols.[19] Rearrangement then occurs to give the product complex **IV**, though the exact nature of the bond rearrangements between **III** and **IV** is unclear. Several proposals have been put forward in the literature, often involving the intermediacy of 2,5-dihydrofuran intermediates, but no definitive studies on the exact mechanism of the rearrangement itself exist[8b,20] Regardless, catalyst turnover is completed by displacement of the product **3** by another molecule of TBHP (**2**). The off-cycle species **I** is in equilibrium with **II**, and both the reversible binding of furfurol (**1**) and product **3** are likely quasiequilibrium steps.

A rate expression for this mechanism derived using the quasiequilibrium assumption and containing only the kinetically meaningful, observed intermediate species may be written as

DOI: 10.1021/jo502641d
J. Org. Chem. XXXX, XXX, XXX−XXX

Table 2. Summary of ^{51}V NMR Chemical Shifts

Entry	Compound	δ (^{51}V)
1	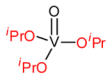	-625
2	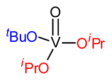	-639
3	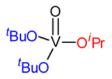	-654
4	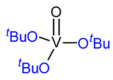 I	-671
8	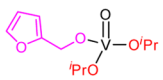	-617
9	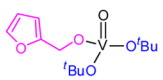	-644
10	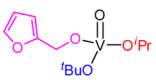	-555
5	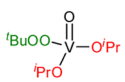	-571
6	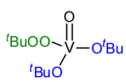 II	-600
7	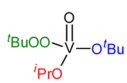	-585
11	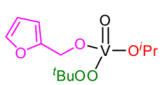	-630
12	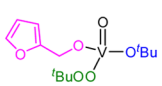 III	-573
13	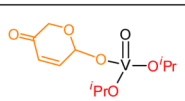	-622
14	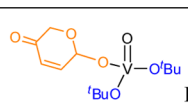 IV	-653

shown in eq 3. The magnitude of the equilibrium constants $K_{eq,1}$ and $K_{eq,4}$ may be estimated from their relative concentrations in Figure 9 at any point during the reaction as shown in eqs 4 and 5. Using these values, the global profile can be fitted to either eq 3 or to the series of elementary steps represented by Scheme 3. This procedure was carried out using the Copasi[21] program and the global kinetic profiles for reaction entries **a**–**c** as shown in Table 1. The global fit also

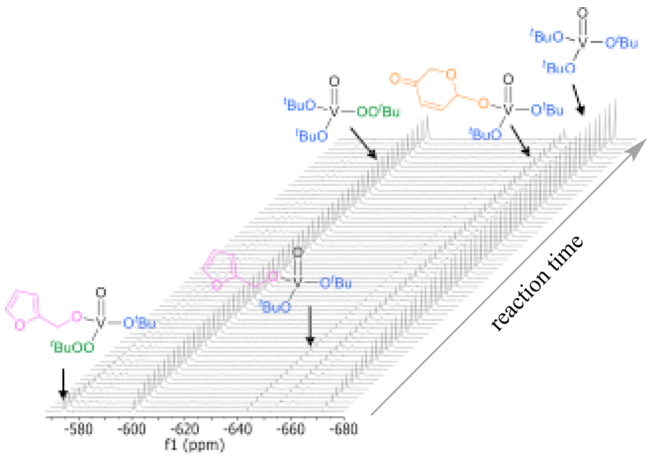

Figure 8. Identification of catalytic species under reaction conditions **h** (Table 1) using $VO(O^tBu)_3$ as catalyst.

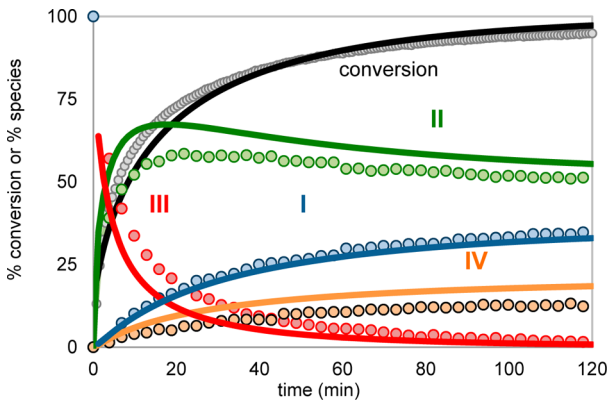

Figure 9. Temporal kinetic profile of reaction catalytic species (%) against time for the reaction of Scheme 1 using $VO(^tBuO)_3$ as the catalyst. Comparison of experimentally observed (symbols) to the simulated (lines) profiles from the mechanism proposed in Scheme 3.

Scheme 3. Plausible Mechanism for the Achmatowicz Rearrangement of Furfurol

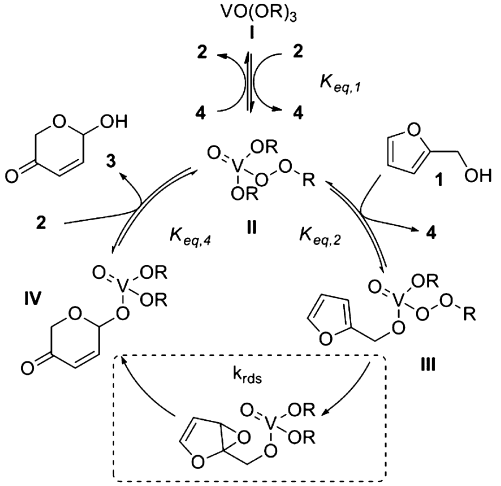

produces a computational prediction of the temporal concentrations for **1** and **3** and the intermediates **I**, **II** **III**, and **IV** and allows for a comparison with the experimentally determined profiles. The model predictions for these intermediates is given by the solid lines of Figure 9. The

DOI: 10.1021/jo502641d
J. Org. Chem. XXXX, XXX, XXX−XXX

good qualitative prediction of the trends for **1**, **3**, and all catalyst intermediates supports this model as a realistic approximation of the catalytic cycle under the reaction conditions. This study offers a rare example of the use of global kinetic data to predict, with fair accuracy, the concentrations of species proposed as catalytic intermediates and observed experimentally. While the reasonable fit to the experimental data shown in Figure 9 cannot preclude other mechanistic possibilities, or even the possibility that these species are not active catalytic intermediates, these combined experimental and kinetic modeling results offer a reasonable rationalization for the catalytic behavior of this system.

$$\text{rate} = \frac{k_{rds}K_{eq,1}K_{eq,2}\frac{[\mathbf{1}][\mathbf{2}]}{[\mathbf{4}]^2}[\text{cat.}]_{total}}{\left(1 + K_{eq,1}\frac{[\mathbf{2}]}{[\mathbf{4}]} + K_{eq,1}K_{eq,2}\frac{[\mathbf{1}][\mathbf{2}]}{[\mathbf{4}]^2} + \frac{K_{eq,1}}{K_{eq,4}}\frac{[\mathbf{3}]}{[\mathbf{4}]}\right)} \quad (3)$$

$$K_{eq,1} = \frac{[\mathbf{II}]}{[\mathbf{I}]}x' - 1 \text{ where } x' = \frac{[\mathbf{2}]_0}{[\mathbf{2}]} \quad (4)$$

$$K_{eq,4} = K_{eq,1}\frac{[\mathbf{I}]}{[\mathbf{IV}]} \text{ where } [\mathbf{3}] = [\mathbf{4}] \quad (5)$$

CONCLUSIONS

A robust and high-yielding method for the Achmatowicz rearrangement of furfurol (**1**) is described which allowed for simple isolation of lactol **3** and its crystalline derivatives. The mechanism of the reaction has been investigated using a combination of ReactIR and ^{1}H and ^{51}V NMR spectroscopy. This has given an increased understanding of the mechanism and elucidation of several important catalytic intermediates. These studies differentiate between *irreversible* catalyst deactivation and *reversible* rate suppression by ^{t}BuOH (**4**), which acts as a competitive ligand impacting the rate of substrate activation and therefore turnover of the productive transformation. From this analysis, it is apparent that the reaction occurs without significant irreversible deactivation of the catalytic species. The increase in concentration of ^{t}BuOH (**4**) is a natural outcome of the productive reaction but is also responsible for the decrease in reaction rate at high conversion. Elucidation of this effect demonstrates that this is fundamentally a robust transformation to generate lactol **3** under conditions applicable to further synthetic manipulations.

EXPERIMENTAL SECTION

General Experimental Methods. $VO(O^iPr)_3$ was stored under nitrogen gas and used as received. For the kinetic studies, furfurol was distilled from potassium bicarbonate and stored over molecular sieves (4 Å) under inert atmosphere. TBHP/decane (~5.5 M) used for kinetic experiments was carefully titrated (×3) with $Na_2S_2O_3$/NaI,[22] and the concentration was found to be 5.42 M. Tri-*tert*-butoxyvanadate was synthesized according to previously reported procedures.[23] 1,3,5-Trimethoxybenzene was employed as the internal standard. In situ FTIR reaction analysis was performed using a ReactIR 45m instrument fitted with a ATR probe. NMR spectra were calibrated using residual proteo-solvent as an internal reference. $VOCl_3$ (neat) was used as an external reference for ^{51}V NMR analysis. In order to obtain quantitative data we measured the 90 deg flip angle (P1/4) and the longitudinal relaxation time (T1) for furfurol.

Preparation of 6-Hydroxy-2*H*-pyran-3(6*H*)-one (3). Anhydrous TBHP was prepared by mixing 8 g (62 mmol, 1.2 equiv) of 70% aqueous *tert*-butyl hydroperoxide (TBHP) together with 20 mL of DCM. The phases were allowed to settle over 1 h, and then the aqueous layer was discarded. The resulting DCM solution of TBHP was used without further purification. To a 250 mL flask under N_2 was added 5.1 g (52 mmol) of furfurol (**1**) along with 80 mL of DCM and 250 μL of $VO(O^iPr)_3$ (1 mmol, 0.02 equiv). The solution was cooled in a room temperature water bath, and the solution of TBHP in DCM was added dropwise over 10 min. Quantitative HPLC analysis indicated 93% conversion, 81% yield after 3 h, at which point residual TBHP was quenched by addition of 0.4 mL of trimethyl phosphite at a rate to maintain the temperature below 30 °C. The reaction mixture was then concentrated under reduced pressure, and 5 mL of *n*-heptane was added followed by 50 mg of pure **3**. After a suspension had formed, 10 mL of *n*-heptanes was added and the suspension aged. The product was isolated via filtration. The cake was washed with 20 mL of 1:1 *n*-heptane/IPA to obtain 3.74 g of 6-hydroxy-2*H*-pyran-3(6*H*)-one as an off-white solid (33 mmol, 63% yield). ^{1}H NMR (500 MHz, $CDCl_3$): 4.14 (d, J = 17.0 Hz, 1 H), 4.36 (d, J = 5.7 Hz, 1 H), 4.57 (d, J = 17.0 Hz, 1 H), 5.63 (dd, J = 5.2, 3.0 Hz, 1 H), 6.17 (d, J = 10.4 Hz, 1 H), 6.98 (dd, J = 10.4, 3.0 Hz, 1 H); ^{13}C NMR (125 MHz, $CDCl_3$): 66.7, 88.3, 127.9, 146.6, 195.3. IR (film): 3308, 1663, 1624, 1278, 1090, 1008, 980, 847, 686 cm^{-1}. HRMS (ESI+): [$C_5H_7O_3^+$] calcd 115.0390, measured 115.0380. Mp: 58−60 °C. Anal. Calcd for $C_5H_6O_3$: C, 52.63; H, 5.30. Found: C, 52.66; H, 5.31.

Preparation of *tert*-Butyl 5-Oxo-2*H*-pyran-2-yl Carbonate (5). In a 250 mL flask, 2.00 g (20.4 mmol, 1 equiv) of furfuryl alcohol was diluted with 40 mL of dichloromethane, followed by the addition of 100 μL (0.408 mmol, 0.02 equiv) of $VO(O^iPr)_3$. The resulting solution was cooled to 10 °C with an ice bath, and 4.5 mL (~5.5 M, 13 mmol, 1.25 equiv) of TBHP in decane was added dropwise over 5 min. The resulting solution was stirred at room temperature. After 4 h, the solution was cooled to 5 °C, and 1.0 mL (8.4 mmol, 0.4 equiv) of trimethyl phosphite was charged dropwise. After completion of the quench, the temperature of the solution was cooled back to 5 °C, and 5.5 g (25.2 mmol, 1.2 equiv) of Boc anhydride was added in one portion, followed by 80 mg (0.67 mmol, 0.03 equiv) of DMAP. ^{1}H NMR analysis at 15 min indicated full conversion. The crude solution was concentrated and purified using column chromatography with EtOAc in hexanes as the eluent. After evaporation of the clean fractions, *tert*-butyl 5-oxo-2*H*-pyran-2-yl carbonate (3.48 g, 15.3 mmol, 75% yield) was isolated as a white solid. ^{1}H NMR (500 MHz, $CDCl_3$): δ 6.87 (dd, J = 10.4, 3.6 Hz, 1H), 6.28 (d, J = 3.6 Hz, 1H), 6.20 (d, J = 10.3 Hz, 1H), 4.50 (d, J = 17.0 Hz, 1H), 4.16 (d, J = 17.0 Hz, 1H), 1.46 (s, 9H). ^{13}C NMR (125 MHz, $CDCl_3$): δ 193.2, 151.8, 141.6, 128.9, 88.8, 83.8, 67.2, 27.7. HRMS (DCI): [$C_{10}H_{15}O_5^+$] calcd 215.0919, measured 215.0921. Mp: 83−85 °C.

Preparation of 5-Oxo-2H-pyran-2-yl 2-Phenylacetate (6). In a 250 mL flask, 1.00 g (10.2 mmol, 1 equiv) of furfuryl alcohol was diluted with 20 mL of dichloromethane, followed by the addition of 50 μL (0.204 mmol, 0.02 equiv) of $VO(O^iPr)_3$. The resulting solution was cooled to 10 °C with an ice bath, and 2.3 mL (~5.5 M, 13 mmol, 1.25 equiv) of TBHP in decane was added dropwise over 5 min. The resulting solution was stirred at room temperature. After 4 h, the solution was cooled to 5 °C, and 0.5 mL (4.24 mmol, 0.4 equiv) of trimethyl phosphite was charged dropwise. After the completion of the quench, the temperature of the solution was cooled back to 5 °C, and 3.20 g (12.6 mmol, 1.2 equiv) of 2-phenylacetyl 2-phenylacetate was added in one portion, followed by 40 mg (0.33 mmol, 0.03 equiv) of DMAP. ^{1}H NMR analysis at 15 min indicated full conversion. The crude solution was concentrated and purified using column chromatography with EtOAc in hexanes as the eluent. After evaporation of the clean fractions, 2.7 g of desired material contaminated with phenylacetic acid was isolated. The material was diluted with 15 mL of ethyl acetate, washed twice with saturated sodium bicarbonate solution, and dried with sodium sulfate to receive 5-oxo-2*H*-pyran-2-yl 2-phenylacetate (1.66 g, 7.15 mmol, 70% yield) as white solid after evaporation. ^{1}H NMR (500 MHz, $CDCl_3$): δ 7.40−7.19 (m, 5H), 6.91 (dd, J = 10.4, 3.6 Hz, 1H), 6.50 (d, J = 3.6 Hz, 1H), 6.26 (d, J = 10.4 Hz, 1H), 4.37 (d, J = 17.0 Hz, 1H), 4.17 (d, J = 17.0 Hz, 1H), 3.69 (s, 2H). ^{13}C NMR (125 MHz, $CDCl_3$): δ 193.3, 170.1, 142.1, 133.1, 129.2, 128.7, 128.7, 127.4, 86.8, 67.2, 41.2. HRMS

DOI: 10.1021/jo502641d
J. Org. Chem. XXXX, XXX, XXX−XXX

(ESI-): [$C_{13}H_{11}O_4^-$] calcd 231.06519, measured 231.06600. Mp: 55−57 °C.

■ ASSOCIATED CONTENT

Supporting Information

Full experimental details and supplementary experiments. This material is available free of charge via the Internet at http://pubs.acs.org.

■ AUTHOR INFORMATION

Corresponding Authors

*E-mail: tamas.benkovics@bms.com.

*E-mail: blackmond@scripps.edu

Notes

The authors declare no competing financial interest.

■ ACKNOWLEDGMENTS

This work was supported by collaboration between Bristol-Myers Squibb Company and The Scripps Research Institute. We thank Drs. David Kronenthal and Joel Barrish for supporting this work.

■ REFERENCES

(1) Georgiadis, M. P.; Albizati, K. E.; Georgiadis, T. M. *Org. Prep. Proc.* **1992**, *24*, 95−118.

(2) (a) Cuccarese, M. F., O'Doherty, G. A. In *Asymmetric Synthesis II: More Methods and Applications*; Christmann, M., Braese, S., Eds.; Wiley−VCH: Weinheim, 2012; pp 249−259. (b) Guo, H. B.; O'Doherty, G. A. *J. Org. Chem.* **2008**, *73*, 5211−5220. (c) Harris, J. M.; Li, M.; Scott, J. G.; O'Doherty, G. A. *Strategies Tactics Org. Synth.* **2004**, *5*, 221−253. (d) Achmatowicz, O.; Bielski, R. *Carbohydr. Res.* **1977**, *55*, 165−176. (e) Achmatowicz, O.; Bukowski, P.; Szechner, B.; Zwierzchowska, Z. *Tetrahedron* **1971**, *27*, 1973−1996.

(3) For representative examples, see: (a) Nicolaou, K. C.; Aversa, R. J.; Jin, J.; Rivas, F. *J. Am. Chem. Soc.* **2010**, *132*, 6855−6861. (b) Zhou, X. F.; Wu, W. Q.; Liu, X. Z.; Lee, C. S. *Org. Lett.* **2008**, *10*, 5525−5528. (c) Jones, R. A.; Krische, M. J. *Org. Lett.* **2009**, *11*, 1849−1851. (d) Abrams, J. N.; Babu, R. S.; Guo, H. B.; Le, D.; Le, J.; Osbourn, J. M.; O'Doherty, G. A. *J. Org. Chem.* **2008**, *73*, 1935−1940. (e) Wender, P. A.; Bi, F. C.; Buschmann, N.; Gosselin, F.; Kan, C.; Kee, J. M.; Ohmura, H. *Org. Lett.* **2006**, *8*, 5373−5376.

(4) (a) Shimokawa, J.; Harada, T.; Yokoshima, S.; Fukuyama, T. *J. Am. Chem. Soc.* **2011**, *133*, 17634−17637. (b) Benkovics, T.; Ortiz, A.; Guo, Z.; Goswami, A.; Deshpande, P. *Org. Synth.* **2014**, *91*, 293−306.

(5) Kolb, H. C.; Hoffmann, H. M. R. *Tetrahedron: Asymmetry* **1990**, *1*, 237−250.

(6) See further discussion on p 106 of ref 1.

(7) (a) Wahlen, J.; Moens, B.; De Vos, D. E.; Alsters, P. L.; Jacobs, P. A. *Adv. Synth. Catal.* **2004**, *346*, 333−338. (b) Finlay, J.; McKervey, M. A.; Gunaratne, H. Q. N. *Tetrahedron Lett.* **1998**, *39*, 5651−5654.

(8) (a) Jackson, K. L.; Henderson, J. A.; Morris, J. C.; Motoyoshi, H.; Phillips, A. J. *Tetrahedron Lett.* **2008**, *49*, 2939−2941. (b) Ho, T. L.; Sapp, S. G. *Synth. Commun.* **1983**, *13*, 207−211.

(9) (a) Blackmond, D. G. *Angew. Chem., Int. Ed.* **2005**, *44*, 4302−4320. (b) Mathew, J. S.; Klussmann, M.; Iwamura, H.; Valera, F.; Futran, A.; Emanuelsson, E. A. C.; Blackmond, D. G. *J. Org. Chem.* **2006**, *71*, 4711−4722.

(10) Rehder, D. In *Multinuclear NMR*; Mason, J., Ed.; Plenum Press: New York, 1987; pp 488−493.

(11) (a) Crans, D. C.; Chen, H.; Felty, R. A. *J. Am. Chem. Soc.* **1992**, *114*, 4543−4550. (b) Hillerns, F.; Rehder, D. *Chem. Ber.* **1991**, *124*, 2249−2254.

(12) Bryant, B. E.; Fernelius, W. C.; Busch, D. H.; Stouffer, R. C.; Stratton, W. *Inorganic Synthesis* **1957**, *5*, 113−116.

(13) (a) Bortolini, O.; Di Furia, F.; Modena, G. *J. Mol. Catal.* **1983**, *19*, 319−329. (b) Su, C.-C.; Reed, J. W.; Gould, E. S. *Inorg. Chem.* **1973**, *12*, 337−342. (c) Gould, E. S.; Hiatt, R. R.; Irwin, K. C. *J. Am. Chem. Soc.* **1968**, *90*, 4573−4579.

(14) Curci, R.; Di Furia, F.; Testi, R.; Modena, G. *J. Chem. Soc., Perkin Trans. 2* **1974**, 752−757.

(15) (a) Adão, P.; Kuznetsov, M. L.; Barroso, S.; Martins, A. M.; Avecilla, F.; Pessoa, J. C. *Inorg. Chem.* **2012**, *51*, 11430−11449. (b) Figiel, P. J.; Sobczak, J. M. *J. Catal.* **2009**, *263*, 167−172. (c) Hartung, J. *Pure Appl. Chem.* **2005**, *77*, 1559−1574. (d) Bryliakov, K. P.; Talsi, E. P. *Kinet. Catal.* **2003**, *44*, 334−346. (e) Smith, T. S.; Pecoraro, V. L. *Inorg. Chem.* **2002**, *41*, 6754−6760.

(16) (a) Bryliakov, K. P.; Talsi, E. P.; Stas'ko, S. N.; Kholdeeva, O. A.; Popov, S. A.; Tkachev, A. V. *J. Mol. Catal. A* **2003**, *194*, 79−88. (b) Talsi, E. P.; Chinakov, V. D.; Babenko, V. P.; Zamaraev, K. I. *J. Mol. Catal.* **1993**, *81*, 235−254.

(17) Vandichel, M.; Leus, K.; Van Der Voort, P.; Waroquier; Van Speybroeck, V. *J. Catal.* **2012**, *294*, 1−18.

(18) (a) Greb, M.; Harung, J.; Koehler, F.; Špehar, K.; Kluge, R.; Csuk, R. *Eur. J. Org. Chem.* **2004**, *18*, 3799−3812. (b) Di Furia, F.; Modena, G.; Curci, R.; Bachofer; Edwards, J. O.; Pomerantz, M. *J. Mol. Catal.* **1982**, *14*, 219−229.

(19) Itoh, T.; Jitsukawa, K.; Kaneda, K.; Teranishi, S. *J. Am. Chem. Soc.* **1979**, *101*, 159−169.

(20) (a) Achmatowicz, O.; Burzynska, M. H. *Carbohydr. Res.* **1985**, *141*, 67−76. (b) Sammes, P. G.; Thetford, D. *J. Chem. Soc., Chem. Commun.* **1985**, 352−353. (c) Pelter, A.; Ward, R. S.; James, D. C.; Kamakshi, C. *Tetrahedron Lett.* **1983**, *24*, 3133−3136. (d) Torii, S.; Tanaka, H.; Anoda, T.; Simizu, Y. *Chem. Lett.* **1976**, 495−498.

(21) Hopps, S.; Sahle, S.; Gauges, R.; Lee, C.; Pahle, J.; Simus, N.; Singhal, M.; Xu, L.; Mendes, P.; Kummer, U. COPASI − A Complex Pathway Simulator. *Bioinformatics* **2006**, *22* (24), 3067−3074.

(22) Verhoeven, T. R.; Sharpless, K. B. *Aldrichimica Acta* **1979**, *12*, 63−74.

(23) Mittal, R. K.; Mehrotra, R. C. *Z. Anorg. Allg. Chem.* **1964**, *327*, 311−314.

DOI: 10.1021/jo502641d
J. Org. Chem. XXXX, XXX, XXX−XXX